The Importance of Metabasic Rocks in Deep Nitrogen Cycling: Insights From Amphibolite and Epidote-Blueschists from the Qiangtang Metamorphic Belt, Central Tibet

Ananya Mallik[a]*, Anna M Rebaza[a], Long Li[b], Yifan Du[b], Ahmed Al Shams[a], Paul Kapp[a], Emily H. G Cooperdock[c]

[a]Department of Geosciences, University of Arizona, 1040 E 4th St., Tucson, AZ 85715, USA

[b]Department of Earth & Atmospheric Sciences, University of Alberta, Edmonton, Alberta, T6G 2E3, Canada

[c]Department of Earth, Environmental and Planetary Sciences, Brown University, Box 1846, 324 Brook Street, Providence, RI 02912, USA

* Corresponding author, email: mallika@arizona.edu, Twitter: @DrRockChef

This preprint has been submitted to Geochimica et Cosmochimica Acta for peer review.

Abstract

Understanding deep nitrogen (N) cycling better requires investigating the inputs of N to subduction systems through various lithologies. Input to subduction zones through mafic rocks is more voluminous and massive as compared to sedimentary rocks which calls for a thorough investigation of the behavior of N in metabasic rocks. Here we investigate the input of N to subduction zones by investigating the geochemistry of amphibolites and epidote-blueschists from the Central Qiangtang Metamorphic Belt in Tibet where the metabasic rocks likely represent the transition from oceanic to continental subduction. The rocks contain 21-147 ppm N with $\delta^{15}N$ values from +1.8‰ to +10.0‰, and 147 ppm N is the highest that has been reported in a metabasic rock thus far. Positive correlations between N and fluid-mobile elements such K, Rb and Ba indicate that N was acquired by the rocks via fluids and the positive $\delta^{15}N$ values indicate that the fluids were sediment or continental derived. Given the N abundances for most of the rocks are much higher than those of mid-ocean ridge basalts and altered oceanic crust (basalts and gabbros), the N is likely neither magmatic nor was introduced in the rocks during hydrothermal alteration prior to subduction. This is confirmed by the K_2O/Th versus Ba/Th, Th/U versus Th and Ba/Rb versus K_2O plots where these rocks align with the trend of metamorphic fluid alteration rather than seafloor hydrothermal alteration. This confirms that these trace elements, along with N, were likely imparted to the rocks during metamorphism within the subduction channel or during underthrusting. We modeled the input fluxes of N in 55 modern-day subduction zones via metasedimentary and metabasic rocks assuming their minimum, median and maximum N concentrations to assess their relative importance in delivery of N to subduction zones. We find that

metabasic rocks supply an overall higher flux of N at forearc depths than metasedimentary rocks, even though metasedimentary rocks have at least an order of magnitude higher N abundance than metabasic rocks. This reinforces the need to investigate the behavior of N in metabasic rocks from more locations globally to improve our understanding of deep N cycling.

1. Introduction

Understanding the behavior of nitrogen (N) in subduction zones is an essential part of deep N cycling. The inputs of N to subduction zones take place through subduction of unmetamorphosed sediments or sedimentary rocks, altered oceanic crust (AOC), intrusive and volcanic rocks, and abyssal serpentinites, as well as through fore-arc processed mélanges that include metasedimentary, metabasic rocks and serpentinized lithosphere (e.g. Bebout and Barton, 2002; King et al., 2003; Cooperdock et al., 2018). To constrain inputs of N through these lithologies better, it is important to assess their N concentrations and the factors which govern these N concentrations.

Metasediments have an order of magnitude higher median concentration of N (360 ppm for n = 155, based on data from Bebout and Fogel, 1992; Bebout, 1997; Busigny et al., 2003, 2005; Sadofsky and Bebout, 2003; Halama et al., 2010; Bebout et al., 2013; Cannaò et al., 2020) as compared to metabasic rocks (10 ppm for n = 118, based on the data from (Halama et al., 2010, 2017; Busigny et al., 2011, 2018; K. Li et al., 2021; this study). This implies that sediments, after dehydration and metamorphism in the accretionary prism or as they enter the subduction channel, retain a higher

concentration of N as compared to mafic rocks (mafic volcanics, oceanic crust) undergoing the same processes. However, mafic input to subduction zones (in the form of oceanic crust or mafic volcanics) is more voluminous than sediments which may lead to metabasic rocks being more effective in carrying N to forearcs and further depths than metasedimentary rocks (K. Li et al., 2021). Therefore, this calls for a thorough investigation of the behavior of N in metabasic rocks.

Previous studies have investigated N behavior in metabasic rocks to understand the processes through which N is acquired by the rock and the behavior of N during metamorphism. Halama et al. (2010) reported 2-20 ppm N ($\delta^{15}N$ = -1‰ to +8‰) in eclogites from the Raspas Complex in Ecuador, Zambezi Belt in Zambia, Lago di Cignana in Italy and Cabo Ortegal in Spain. These eclogites had a range of N characteristics including a few that were nearly identical to altered oceanic crust (AOC), a few that had undergone effects of devolatilization, as well as few that had metasomatic additions during subduction-zone metamorphism. Halama et al. (2017) measured N contents and isotope compositions ($\delta^{15}N$ = +1.0‰ to +5.4‰) in the blueschists and eclogites from Tianshan, China and observed a systematic decrease in N concentrations from blueschist (~26 ppm), to blueschist-eclogite transition zone (19-23 ppm) to eclogite (12-16 ppm) which they interpreted as a product of batch devolatilization process during metamorphism. Harris et al., (2022) reported the first in-situ measurements of N concentrations in phengite and chlorite within blueschists and eclogites from Lago di Cignana in Italy, Raspas Complex in Ecuador and Franciscan Complex in north-west California. They found that, while phengite is the principal host of

93 N, chlorite has variable N abundance and maybe one of the key players in N cycling via
94 metabasic rocks. The study also demonstrated the complexity in the mobility of N during
95 subduction with not only fluid-rock interactions but redistribution of N between minerals
96 (such as between phengite and pargasite) being important. Busigny et al. (2011, 2018)
97 analyzed N concentrations (2.6 – 55 ppm) and isotope compositions ($\delta^{15}N$ = +0.8‰ to
98 +8.1‰) in the metabasic rocks from the Western Alps such as greenschists and
99 amphibolites from the Chenaillet Massif in France, blueschists from the Queyras region
100 in France and eclogites from the Monviso Massif in Italy. Using Cu concentrations and
101 $\delta^{65}Cu$ as tracers, they inferred that N was leached out from those metabasic rocks
102 during hydrothermal alteration although this interpretation has been challenged by L. Li
103 et al., (2021a). Finally, K. Li et al. (2021) reported the N abundances (14 – 122 ppm)
104 and isotope compositions ($\delta^{15}N$ = -10.9‰ to +3.7‰) in the blueschists from the
105 Heilongjiang Complex in Northeastern China. This is the first study that reported N
106 concentrations >100 ppm in metabasic rocks and based on the N concentrations being
107 higher than that in AOC, they inferred that N was introduced mostly in the subduction
108 channel from released N from metasediments during metamorphism. In summary,
109 previous studies that have analyzed metabasic rocks for N inferred more than one
110 process of N incorporation ranging from inheritance due to hydrothermal alteration at
111 the seafloor, to hydrothermal leaching or devolatilization during metamorphism, to
112 addition of N during metamorphism in the subduction channel. Depending on the
113 process, the N abundances and isotopic signatures vary widely across metabasic rocks
114 from the regions mentioned above and thus the inputs of N to subduction zones can
115 vary widely. This calls for further investigation of N characteristics in metabasic rocks

from other regions to expand on the database of N inputs by metabasic rocks and especially assess if one or more processes of N acquisition as inferred by the previous studies represent specific-case scenarios or are generally representative of subduction zones globally.

Nitrogen characteristics (abundance and isotopes) in metabasic rocks depend on (a) the formation conditions of the protoliths and (b) the processes that lead to N inheritance in the metabasic rocks. While previous studies have investigated metabasic rocks whose protoliths consist of seafloor basalts representing AOC or gabbros from lower oceanic crust (e.g. Halama et al., 2010; K. Li et al., 2021), mafic magmatism associated with transition from oceanic to continental subduction remain an uninvestigated lithology in terms of assessing their potential to contribute N to subduction zones.

In this study, we investigate the input of N to subduction zones by focusing on their delivery by metabasic rocks (amphibolites and epidote-blueschists) from the Central Qiantang Metamorphic Belt (CQMB) in Tibet where the mafic magmatism likely represents transition from oceanic to continental subduction. We analyze N abundances and isotope compositions, as well as trace elements in the samples to understand the process of N acquisition. We use N abundances for metasedimentary and metabasic rocks from this study and those reported in the literature to assess the relative contributions of metasedimentary versus metabasic rocks to deep N cycling.

2. Geological Background and samples

2.1 Geological Background

Tibet consists of the Kunlun-Qaidam terrane, the Songpan-Ganzi flysch complex, the North and South Qiangtang terrane(s) and the Lhasa terrane from north to south (Fig. 1). The epidote-blueschists and amphibolites studied here are from three locations in the central Qiangtang metamorphic belt – Gangma, Rongma and Shuang Hu from the west to the east. These metabasites are part of a tectonized mélange with dominantly siliciclastic metasedimentary matrix with blocks and tectonized slivers that include Paleozoic-Triassic strata, sandstone, marble, ophiolitic rocks and amphibole-, blueschist- and eclogite-facies metabasites and schists (Kapp and Decelles, 2019 and references therein). The high-pressure metamorphism in the mélange took place between 244 and 230 Ma during either the southward subduction of the Paleo-Tethys ocean beneath the Qiangtang terrane (Kapp et al., 2003; Pullen et al., 2008) or dominantly northward subduction of an ocean basin between the South and North Qiangtang terranes (Li et al., 1995; Zhang et al., 2006; Wu et al., 2016). Recognition of metamorphosed upper Paleozoic Qiangtang continental margin strata and fragments of continental basement in the CQMB raise the possibilities that oceanic subduction tectonically eroded the upper continental plate (Kapp et al., 2003; Zhang et al., 2017) and/or was transitioning into continental margin subduction (Zhang et al., 2006; Xu et al., 2021). Metabasites in the CQMB consist of both blocks and strongly-sheared matrix within a sediment-rich block-in-matrix mélange (e.g., Kapp et al., 2003). Geochemical studies are generally consistent with CQMB metabasites having an oceanic crustal protolith (E-MORB and OIB affinity; Zhai et al., 2011; Dan et al., 2018), although other

protoliths including mafic sills and lavas in upper Paleozoic rifted continental margin strata that were subducted and inter-mixed with CQMB mélange cannot be precluded (Kapp et al., 2003; Pullen et al., 2008; Zhang et al., 2017; Xu et al., 2021). Everywhere studied in detail, high-P rocks of the CQMB were exhumed structurally beneath lower-grade upper Paleozoic – Triassic Qiangtang continental margin strata in the footwalls of domal low-angle normal faults (between ~ 225 and 204 Ma; Kapp et al., 2000, 2003; Liang et al., 2017). This structural setting requires the CQMB rocks to have underplated the Qiangtang continental margin, presumably during a phase of relatively shallow-depth flat-slab subduction (Kapp et al., 2003).

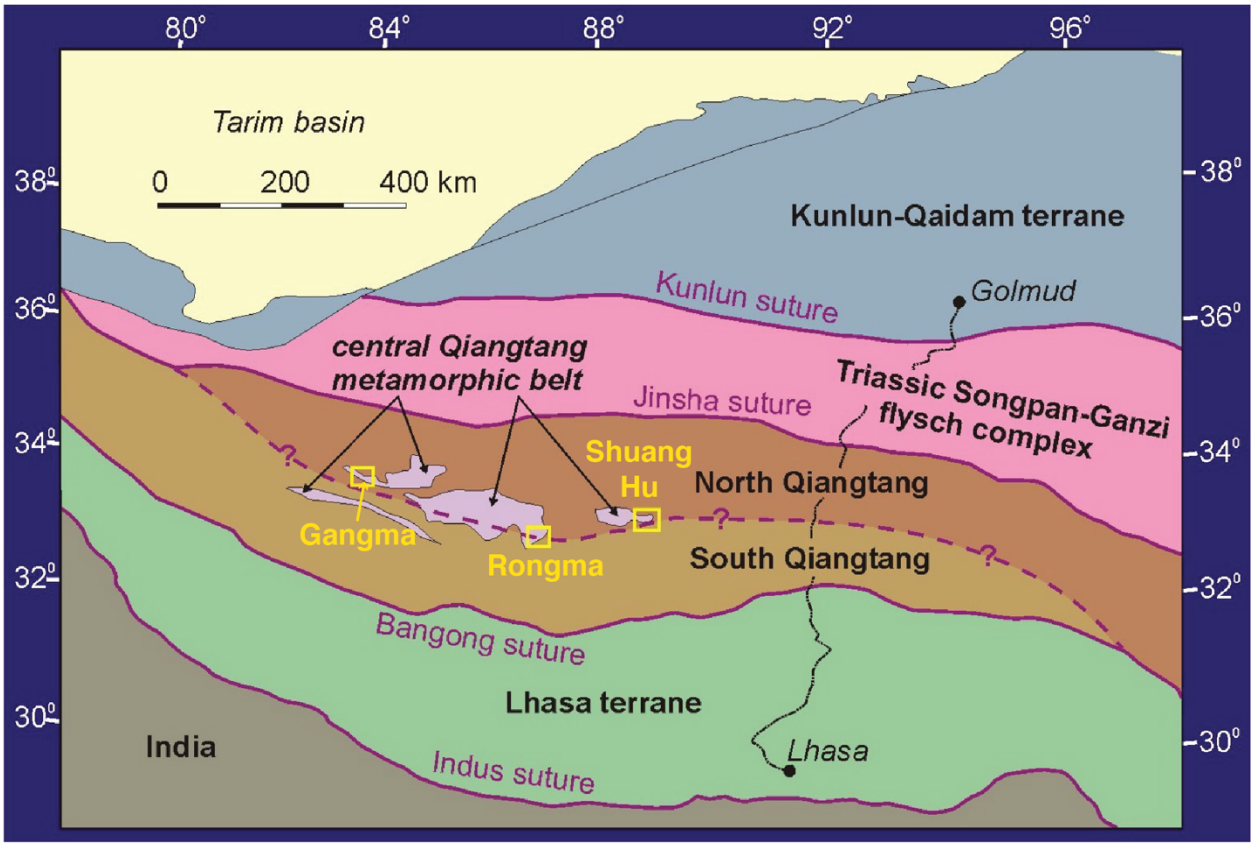

Figure 1. Geological map of Tibet (modified from Kapp et al., 2003). Yellow boxes show areas from which samples have been studied here.

2.2 Samples

We analyzed four amphibolite blocks from Shuang Hu and two strongly-sheared matrix epidote blueschists from each of the three localities (Rongma, Shuang Hu and Gangma). While Gangma and Rongma are about 280 km apart, Rongma and Shuang Hu are about 165 km apart. The petrography for all the samples were previously reported by Kapp et al., (2003). The epidote blueschists from Shuang Hu and Gangma show signs of retrogression, including green amphibolite (actinolite) rims or overgrowths on blue amphibole (glaucophane) and fine-grained crystallization of matrix chlorite. The amphibolites from Shuang Hu and epidote blueschists from Rongma do not show any signs of retrogression. We selected a few potentially retrogressed samples along with unretrogressed ones to assess whether the process of retrogression may impart any systematic geochemical signature in terms of nitrogen abundance and isotopes.

Petrographic images of the samples from this study are included in Supplementary Information. The epidote blueschists contain plagioclase, chlorite, quartz, epidote, blue amphibole (glaucophane), clinopyroxene, sphene, with or without muscovite, calcite, rutile, ilmenite and apatite. Biotite (a potential key N hosting mineral) is remarkably absent from the epidote blueschists. Garnet is absent from all but one (Sample 6-30-99-2D) epidote blueschist. As discussed previously, the effect of retrogression is visible by the rimming of glaucophane by actinolite. The amphibolites contain plagioclase, quartz, epidote, hornblende, biotite, sphene, rutile, with or without chlorite, calcite, clinopyroxene, garnet, Fe-Ti oxide, apatite and pyrite. Muscovite (another potentially key N hosting mineral) is remarkably absent from all the amphibolites.

Kapp et al., (2003) performed thermobarometry on these rocks. The study determined a peak condition of 11 kbar, 660 ℃ for the amphibolites (using the hornblende-plagioclase thermometry of Holland and Blundy, 1994 and garnet-hornblende-plagioclase barometry of Kohn and Spear, 1990) and 10-14 kbar, 350-525 ℃ for the epidote blueschists (using the phengite barometer of Massonne and Schreyer, 1987 and chlorite-muscovite thermometer of Powell and Evans, 1983 and Bucher-Nurminen, 1987). Subsequent pseudosection modeling of Rongma epidote blueschists, however, suggests higher peak-P conditions of ~23 kbar at ~550 ℃ (Xu et al., 2021).

3. Analytical methods

3.1 Major and trace elements

Bulk chemical analysis on all samples was done by Wavelength Dispersive X-Ray Fluorescence (WDXRF) at Hamilton Analytical Lab. WDXRF determinations were made with low-dilution (1:2 sample to flux ratio with Li-tetraborate only) doubly fused glass beads made using an adaptation of the preparation method described by Johnson et al. (1999); the usual mass of each sample is 3.5 grams for a 29 mm bead, less for a 15 mm bead. The chief difference is in the use of diamond polishing, rather than SiC grit, to create the analytical surface. First fused beads are re-ground to powder in a tungsten carbide ringmill for 30 seconds and fused again; both fusions occur under static conditions in a 1000 °C muffle furnace. The flat surface of the doubly fused bead was ground to a 15 μ finish on diamond lapping plates and sonicated in ethanol before set for analysis in the WDXRF spectrometer.

For WDXRF determinations, single backgrounds for each element were measured, and background was subtracted with formulas derived from pure element spike experiments. Equal time was spent counting peak and background positions for all elements. Total analytical time per bead was approximately 130 minutes. All intensities were collected at 45 kV and 45 mA. Spectral interferences were corrected with net intensity ratio factors or formulas derived from experiments with pure element spikes doped into either SiO_2 or Al_2O_3 matrices. LOI-eliminated influence coefficients were used for matrix correction. Calibration was done using the intensities gathered from 77 CRMs and RMs, chiefly those issued by the USGS and GSJ, but also including RMs from the CRPG, GIT-IWG, NIST, BAS, Mintek, and other sources. The revised USGS, GSJ, and CRPG CRM values provided in Jochum et al., (2016) were used and weighted more heavily than the values from other CRMs. Repeated analysis of internal standards and samples gave an analytical error (2σ) of ≤6% of the absolute value for major and minor elements and 1-215% for trace elements (the highest error is for Cs).

Further details of the calibration procedure and validation of the WDXRF method can be accessed at *https://www.hamilton.edu/academics/analytical-lab*.

3.2 Nitrogen abundance and isotopes

Nitrogen concentrations and isotope compositions were analyzed at University of Alberta following the technique by L.Li et al. (2021b). Sample powders were loaded together with CuO reagent and quartz wool in a one end-sealed quartz tube, which was put on a metal manifold to pump overnight. The sample tube was then sealed under high vacuum and combusted at 900 °C for 8 hours followed by 600 °C for 2 hours for a

complete extraction of N in the blueschist samples and turning it into N_2 (L. Li et al., 2021b). The sample tube was subsequently cracked in a tube cracker in the metal manifold under high vacuum. The N_2 product was cryogenically purified, quantified by a capacitance manometer, and sent by a high-purity helium stream to a Thermo Finnegan MAT 253 isotope ratio mass spectrometer for isotopic analysis. Repeated analysis of internal standards and samples (all calibrated by two OAS reference materials LOCS and HOSC) gave an analytical error (2σ) of <5% of the absolute value for N concentrations and <0.2‰ for δ^{15}N values.

4. Results

4.1 Trace elements and nitrogen geochemistry

We report the bulk major and trace element chemistries along with N abundances and isotopic ratios of the samples in Table 1.

We obtained 14-147 ppm N and δ^{15}N values from +1.8‰ to +10.0 ‰ in the metabasic rocks from this study (Fig. 2). The Shuang Hu amphibolites show a range of N abundance from 21 – 147 ppm and δ^{15}N values from +3.1‰ to +9.1‰. The Rongma epidote blueschists show a range of N abundance from 14 – 43 ppm and δ^{15}N values from +1.8‰ to +8.0‰. The two retrogressed epidote blueschists from Shuang Hu show N abundances of 24 and104 ppm, and δ^{15}N values of +5.7‰ and +7.2‰. The two retrogressed epidote blueschists from Gangma show N abundances of 44 and 93 ppm and δ^{15}N values of +3.7‰ and +10.0‰. We observe positive correlations between N and K_2O, N and Rb, and N and Ba abundances (Fig. 2).

Table 1. Compositions of metabasic rocks from this study

SampleID	5-30-98-11F	Repeat	5-30-98-11E	Repeat	6-13-97-3A	97-6-16-4A	97-6-16-4B	6-13-97-3B	97-6-14-1PK	5-30-99-4	5-28-99-4B	6-13-97-2	6-30-99-2D	Repeat
Rock type	E-BS-R		E-BS-R		A	A	A	A	A-R	E-BS	E-BS	E-BS-R	E-BS	
Location	Matrix, foliated Gangma		Matrix, foliated Gangma		Block, foliated Shuanghu	Block, foliated Shuanghu	Block, foliated Shuanghu	Block, weakly foliated Shuanghu	Matrix, foliated Shuanghu	Matrix, undeformed Rongma	Matrix, weakly foliated Rongma	Matrix, undeformed Shuanghu	Matrix, foliated Rongma	
N (ppm)	44.0	44.3	93.2	98.3	91.1	21.0	27.5	147.3	23.8	42.7	41.4	103.7	14.4	14.1
$\delta^{15}N$ ‰	10.0	9.7	3.7	3.7	5.6	6.6	9.1	3.1	5.7	3.7	1.8	7.2	8.0	8
SiO_2 (wt.%)	45.8		46.5		47.6	47.2	49.2	40.5	42.9	45.4	42.6	45.8	44.7	
TiO_2	4.2		3.4		1.3	2.3	0.2	6.3	4.4	4.5	3.5	4.4	2.9	
Al_2O_3	10.3		10.6		12.0	13.2	16.4	10.6	6.2	15.6	8.6	10.3	8.1	
FeO	7.9		7.0		7.8	7.3	2.9	9.1	8.1	8.1	7.8	8.4	7.9	
Fe_2O_3	4.9		4.2		4.0	5.1	1.3	4.8	5.0	4.2	5.1	4.7	4.7	
MnO	0.2		0.1		0.2	0.1	0.1	0.2	0.2	0.2	0.2	0.2	0.2	
MgO	8.8		7.2		12.4	6.9	10.6	6.3	15.0	4.0	13.2	9.0	9.0	
CaO	9.9		10.9		7.0	9.0	14.8	11.4	10.5	9.2	11.0	9.5	8.3	
Na_2O	2.5		2.6		1.0	3.4	1.6	1.9	0.6	3.2	1.7	2.5	4.9	
K_2O	2.0		2.7		0.7	0.7	0.4	2.9	0.8	1.3	1.0	1.1	0.0	
P_2O_5	0.5		0.4		0.1	0.8	0.0	1.8	0.5	0.3	0.5	0.6	0.0	
LOI	2.9		3.7		4.7	2.3	1.5	2.4	4.8	2.6	4.1	2.6	6.4	
F (ppm)	830.9		629.6		738.0	719.5	238.8	1890.1	1288.8	555.8	1147.1	931.1	643.9	
Cl	91.4		20.9		193.0	386.0	71.5	46.5	28.8	65.2	87.5	22.8	19.6	
Br	1.5		1.9		2.1	2.0	0.9	2.2	2.4	2.2	1.6	2.4	2.4	
As	3.5		2.8		28.7	3.5	0.0	0.0	0.0	0.0	0.0	6.8	0.0	
S	241.3		96.2		260.0	4830.6	101.1	284.0	110.7	114.3	115.4	623.5	306.8	
Ni	151.0		137.5		261.8	19.8	132.0	21.6	663.9	56.7	538.2	244.0	52.4	
Cr	287.8		282.0		943.3	63.1	1252.8	0.0	1252.0	0.0	1021.2	420.5	53.4	
V	346.1		335.7		270.8	95.8	157.8	539.7	311.2	727.4	315.7	363.9	285.2	

Sc	32.5	25.4	29.1	36.6	43.9	30.3	29.1	33.5	29.0	26.6	33.9
Cu	54.6	103.2	103.2	6.4	63.3	113.6	113.1	159.1	124.6	157.7	34.1
Zn	79.0	53.2	53.7	71.2	0.0	111.2	82.1	75.3	68.9	90.6	108.1
Ga	21.7	20.9	15.2	22.2	9.2	28.1	16.4	23.0	17.3	23.1	12.3
Ba	343.5	645.2	205.3	110.3	17.7	1204.2	221.4	257.1	470.8	310.4	9.0
Rb	42.5	56.0	21.8	13.5	8.4	81.3	24.7	31.9	23.0	33.7	0.5
Cs	0.0	0.8	0.0	3.0	0.0	0.0	1.7	11.6	0.0	1.2	0.0
Sr	358.0	399.4	222.1	121.8	149.9	1381.0	166.6	533.9	308.8	217.7	88.8
Y	31.1	26.4	17.7	71.5	9.1	54.2	24.5	25.3	27.2	32.4	16.2
Zr	327.3	246.6	89.3	358.4	13.7	816.0	383.4	156.2	269.7	384.2	86.1
Hf	8.6	5.2	1.8	9.3	0.4	20.7	9.2	3.8	7.8	9.5	2.3
Nb	48.3	37.3	5.5	33.5	0.0	134.7	71.1	22.1	46.6	67.1	4.9
Ta	4.7	4.5	0.0	6.7	2.2	11.9	5.8	1.1	1.6	7.2	4.4
Mo	3.3	2.0	0.7	2.4	1.5	5.0	2.0	1.8	1.7	2.0	0.6
La	46.4	29.5	13.2	37.0	0.0	149.1	65.2	18.2	42.5	64.4	30.9
Ce	112.8	69.9	26.3	98.3	9.1	345.6	151.0	44.5	93.5	141.3	56.6
Nd	56.8	38.7	15.1	51.6	4.4	172.2	72.9	24.2	45.4	67.1	23.0
Th	7.8	5.1	4.2	11.0	1.3	22.1	10.3	3.5	4.0	6.4	1.0
U	3.3	4.1	1.0	2.5	0.0	7.1	4.9	4.3	4.2	3.6	1.4
Pb	3.6	4.0	4.6	6.0	2.0	12.1	3.8	0.0	0.6	8.7	1.5
Tl	0.0	1.5	3.2	1.2	0.2	0.0	0.0	1.0	0.0	2.7	2.1

'repeat' - repeat analyses of N concentration and isotope of samples 5-30-98-11F, 5-30-98-11E, 6-30-99-2D; SiO_2 to LOI reported in wt.%; F to Tl reported in ppm; 'E-BS' - Epidote blueschist; 'R' - retrogressed; 'A' - Amphibolite

5. Discussion

5.1 Nitrogen addition by metamorphic fluids

We obtained 14-147 ppm N and $\delta^{15}N$ from +1.8‰ to +10.0 ‰ in the metabasic rocks from this study (Fig. 2). The measured N abundance of 147 ppm in the mafic amphibolite from Shuang Hu is the highest reported for metabasic rocks thus far (Halama et al., 2010; Busigny et al., 2011; K. Li et al., 2021). The N concentrations in the amphibolites and epidote blueschists are overall higher than those reported for mid-ocean ridge basalts or altered oceanic crust where the median abundance is 6.0 ± 4.7 ppm (Busigny et al., 2005, 2019; Li et al., 2007; Bebout et al., 2018; Li and Li, 2022, 2023b, a) which likely implies that most of the N is neither magmatic nor was introduced during hydrothermal alteration of mafic layers at passive margins, but was rather introduced by metamorphic fluids either during underplating or in the subduction channel. Retrogressed samples do not show systematically higher or lower N abundances, hence the effect of retrogression during exhumation on N behavior is not clear from this study. The positive correlations between N and K_2O as well as N and Rb (Fig. 2) confirm that N is mostly hosted as NH_4^+ in the silicate minerals by substituting for K^+ or Rb^+, given they have similar ionic radii (NH_4^+ = 1.54 Å from Sidey, 2016; K^+ = 1.65 Å and Rb^+ = 1.75 Å from Shannon, 1976) and the same ionic charge of +1 (e.g. Busigny and Bebout, 2013). The positive correlation between N and Ba abundances (Fig. 2) and that Ba abundances (Table 1) in eight of these rocks are higher than that of N-MORB (19.6 ppm; Gale et al., 2013) and E-MORB (125.5 ppm; Gale et al., 2013) indicate that N was likely transported into the rocks by fluids. These correlations were

also observed in the metabasic rocks studied by Busigny et al. (2011) and K. Li et al. (2021).

To confirm that most of the N in the metabasic rocks was acquired by metamorphic fluids, we also examined their trace element systematics to understand whether the trace element characteristics align with the effects from metamorphic fluids. As compared to hydrothermal alteration on the seafloor, metamorphism results in lowering of K_2O, thus in a plot of K_2O/Th versus Ba/Th, metamorphic fluid alteration results in a lower slope than seafloor hydrothermal alteration (Bebout, 2007). Also, Th is added to the system by metamorphic fluids resulting in Th enrichment and a shallower slope in Th/U versus Th space as compared to seafloor hydrothermal alteration (Bebout, 2007). Both K_2O and Rb are enriched during seafloor hydrothermal alteration but not as much Ba, due to the lower mobility of Ba in hydrothermal fluids compared to K and Rb while Ba may be as mobile as Rb in metamorphic fluids (e.g. Seyfried et al., 1998). Thus in a plot of Ba/Rb versus K_2O, hydrothermal fluids show a decreasing slope while metamorphic fluid alteration shows a flat trend (van der Straaten et al., 2012). In plots of Ba/Rb versus K_2O, K_2O/Th versus Ba/Th, and Th/U versus Th, the metabasic samples from this study lie along the trends for metamorphic fluid alteration (Fig. 3) indicating that the trace element signatures in the metabasic rocks were inherited during metamorphism in the subduction channel rather than on the seafloor. Thus, it is more likely that the N signatures (both in terms of concentration and isotopic ratio) of these metabasic rocks could have been imprinted in the subduction channel during metamorphism rather than during hydrothermal alteration prior to subduction. This observation is similar to that of the blueschist rocks from the Heilongjiang Complex in

318 northeast China (K. Li et al., 2021). The $\delta^{15}N$ being positive for the rocks indicate that
319 the fluids that carried N were likely sourced from metasediments in the subduction
320 channel or even the continental basement.
321
322 We observe a lack of correlation between N abundances and metamorphic
323 temperatures in the samples from this study, in the sense, N abundances are not
324 systematically higher or lower for higher (epidote blueschist) or lower (amphibolite)
325 metamorphic temperatures. We can thus infer that the N abundances are not a result of
326 progressive devolatilization during increasing metamorphic temperatures. Also, the
327 amphibolites from Shuang Hu show a range of N concentrations from 21 – 147 ppm
328 which is indicative of fluid-rock interactions imparting N heterogeneously at a local
329 scale, similar to that observed by K. Li et al. (2021).

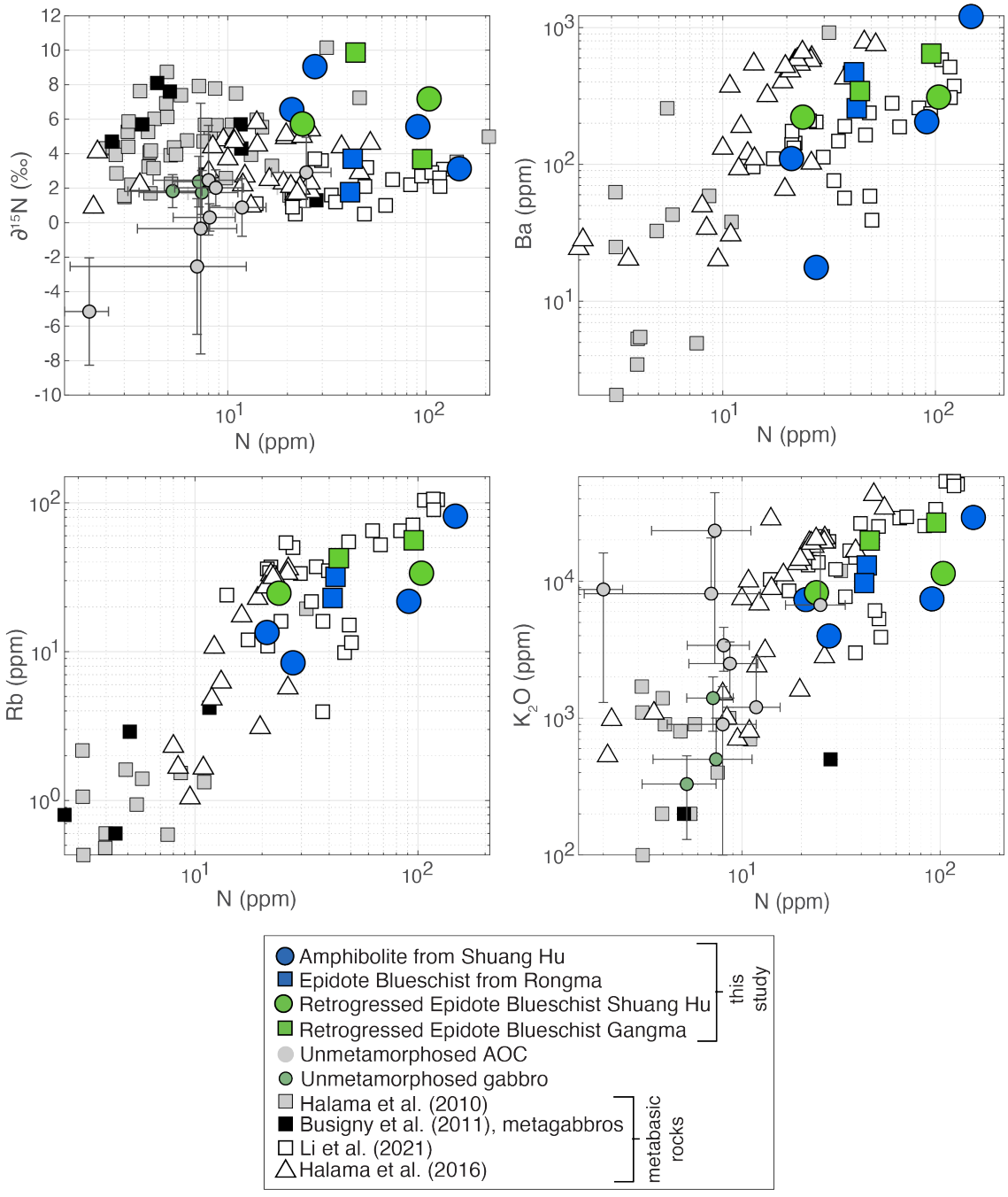

330

331 *Figure 2.* $\delta^{15}N$, Ba, Rb, K_2O versus N for metabasic rocks from this study along with unmetamorphosed altered oceanic crust and
332 metabasic rocks reported by previous studies. Major and trace element concentrations for subducted-metabasic rocks are from
333 Tianshan Belt (Beinlich et al., 2010; van der Straaten et al., 2012), Raspas Complex and Cabo Ortegal (Halama et al., 2010),
334 Zambezi Belt (John et al., 2004), Piemonte-Ligurian domain in western Alps (Busigny et al., 2011), Heilongjiang complex (K. Li et
335 al., 2021). $\delta^{15}N$ (‰) and N concentrations (ppm) in metabasic rocks are from Tianshan Belt (Halama et al., 2017), Piemonte-
336 Ligurian domain in western Alps (Busigny et al., 2011), Heilongjiang complex (K. Li et al., 2021), Raspas Complex, Lago di
337 Cignana, Zambezi Belt, and Cabo Ortegal (Halama et al., 2010). $\delta^{15}N$ (‰), N and K_2O concentrations (average and one-sigma
338 standard deviation) of unmetamorphosed AOC are from Sites 801 and 1149 (Li et al., 2007), Hole 504B (Busigny et al., 2019),
339 ODP Site 1256 (Bebout et al., 2018; Busigny et al., 2005; Li & Li, 2022), Holes 1224F, 543A, 417A, and 556 (Li & Li, 2023b). $\delta^{15}N$
340 (‰), N and K_2O concentrations (average and one-sigma standard deviation) of unmetamorphosed gabbros are from Holes
341 735B, 1309D and 1415P (Li and Li, 2023a).

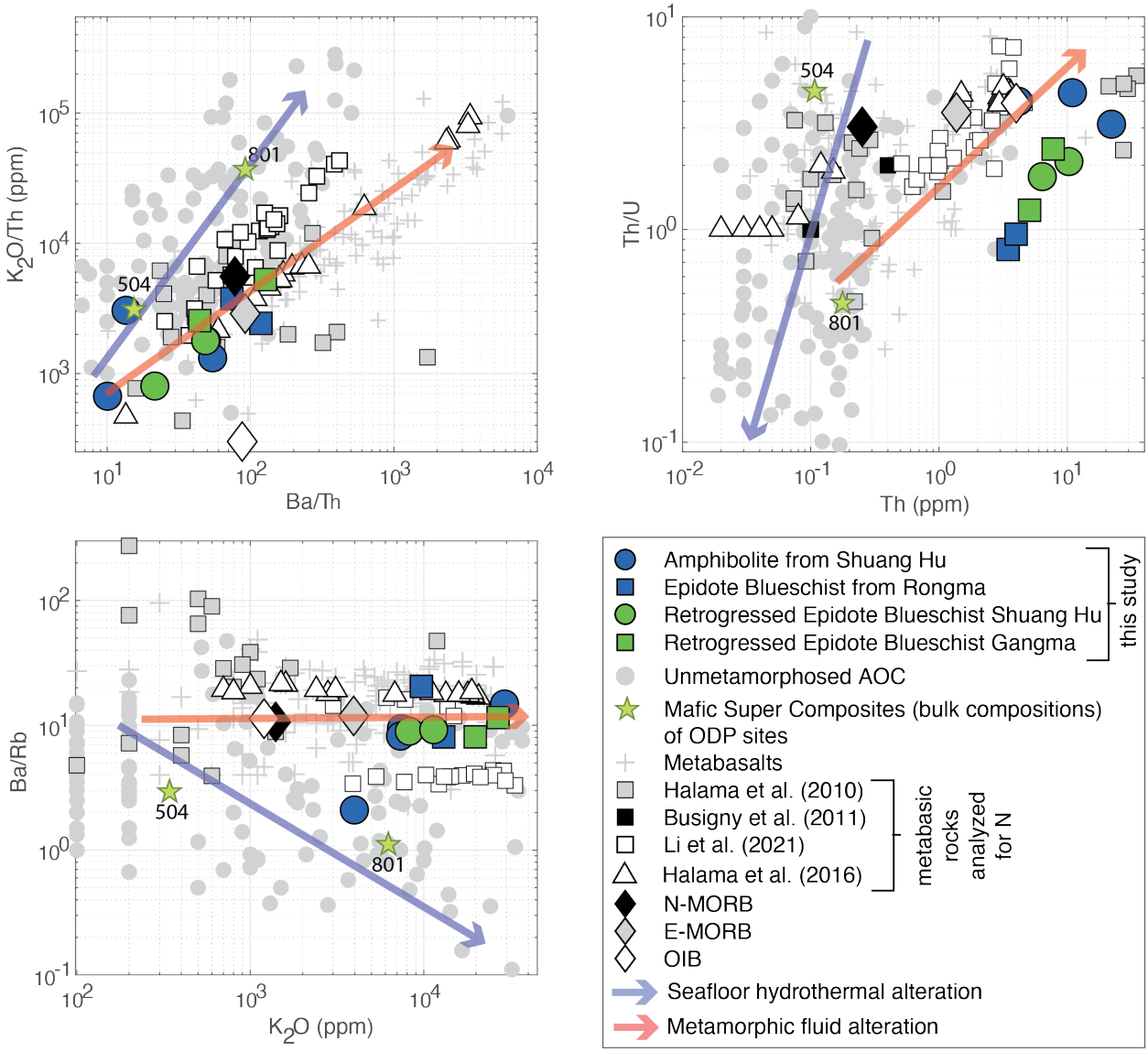

342

343 *Figure 3*. K_2O/Th versus Ba/Th, Th/U versus Th and Ba/Rb versus K_2O for metabasic rocks from this study along with
344 unmetamorphosed altered oceanic crust, metabasalts, and metabasalts that have been analyzed for nitrogen (Halama et al.,
345 2010, 2017; Busigny et al., 2011; K. Li et al., 2021). The unmetamorphosed AOC data including both discrete and super
346 composite data (seafloor hydrothermal alteration) are retrieved from ODP sites 801 and 1149 (Kelley et al., 2003), site 504
347 (Bach et al., 2003). The subduction-related metabasalts (metamorphic fluid alteration) are from the Zambezi Belt (John et al.,
348 2004), Tianshan belt complex (Beinlich et al., 2010; van der Straaten et al., 2012), and Franciscan and Samana Complex
349 (Sorensen et al., 1997). Also plotted are N-MORB (Gale et al., 2013), E-MORB (Gale et al., 2013) and OIB (Sun and
350 McDonough, 1989) for reference.The seafloor hydrothermal and metamorphic fluid alteration trends are based on Bebout,
351 (2007) and van der Straaten et al., (2012).

352

353

354

355 *5.2 Significance of metabasic rocks in delivering nitrogen to forearc conditions*

356 We modeled the input of N by metasedimentary and metabasic rocks in 55 present-day
357 subduction zones (Syracuse et al., 2010; van Keken et al., 2011) to assess the relative
358 importance of metabasic rocks as compared to metasedimentary rocks as agents of
359 nitrogen delivery to forearc conditions within the subduction channel. We assume that
360 all sediment that enters the trench is subducted and the consequences of unsubducted
361 sediments in accretionary prism are discussed towards the end of this section. Even
362 though N may be introduced in subduction zones by mafic rocks other than oceanic
363 crust (such as those associated with volcanism in intracontinental margins), in this
364 section we only consider N delivery by mafic oceanic crust during subduction of oceanic
365 plate beneath oceanic or continental plates. This is simply because the mass of oceanic
366 crust being subducted globally is better constrained whereas the mass of mafic
367 volcanics being subducted through continental subduction and also recycling rates in
368 the mantle due to continental subduction are currently poorly quantified (e.g. Ducea,
369 2016). Towards the end of this section, we discuss how ignoring mafic rocks via
370 continental subduction in our model would have no effect on our findings. We also do
371 not consider inputs of N via serpentinized lithosphere in this study since the degree of
372 serpentinization in the lithosphere is poorly constrained across subduction zones and
373 we choose to avoid adding more uncertainty to our estimates.

374

375 We use subduction velocities, subduction lengths, and sediment thicknesses for each
376 subduction zone segment from van Keken et al., (2011) to calculate the volume of
377 sediment entering each trench. We assume densities of sediments entering each

subduction zone from Plank and Langmuir (1998), except for Calabria where the mean sediment density is taken from Ocean Drilling Program Leg 107 drillsite 650 (Kastens et al., 1987). The oceanic crust is assumed to be 7 km thick, with 600 m of extrusives at the top, followed by 1.4 km of sheeted dikes and gabbro as the remainder (Jarrard, 2003) for each subduction zone segment considered here. In order to account for mass loss during dehydration of sediments during forearc processing, mélange formation and metamorphism (including H_2O, N, Si, Al etc.), and internal distribution of the mass (i.e. uptake of the sediment-derived mass by mafic lithologies), we assume a 25% loss of mass in sediments (based on the lower estimate of Ague, 2011) and add that mass to metabasic rocks.

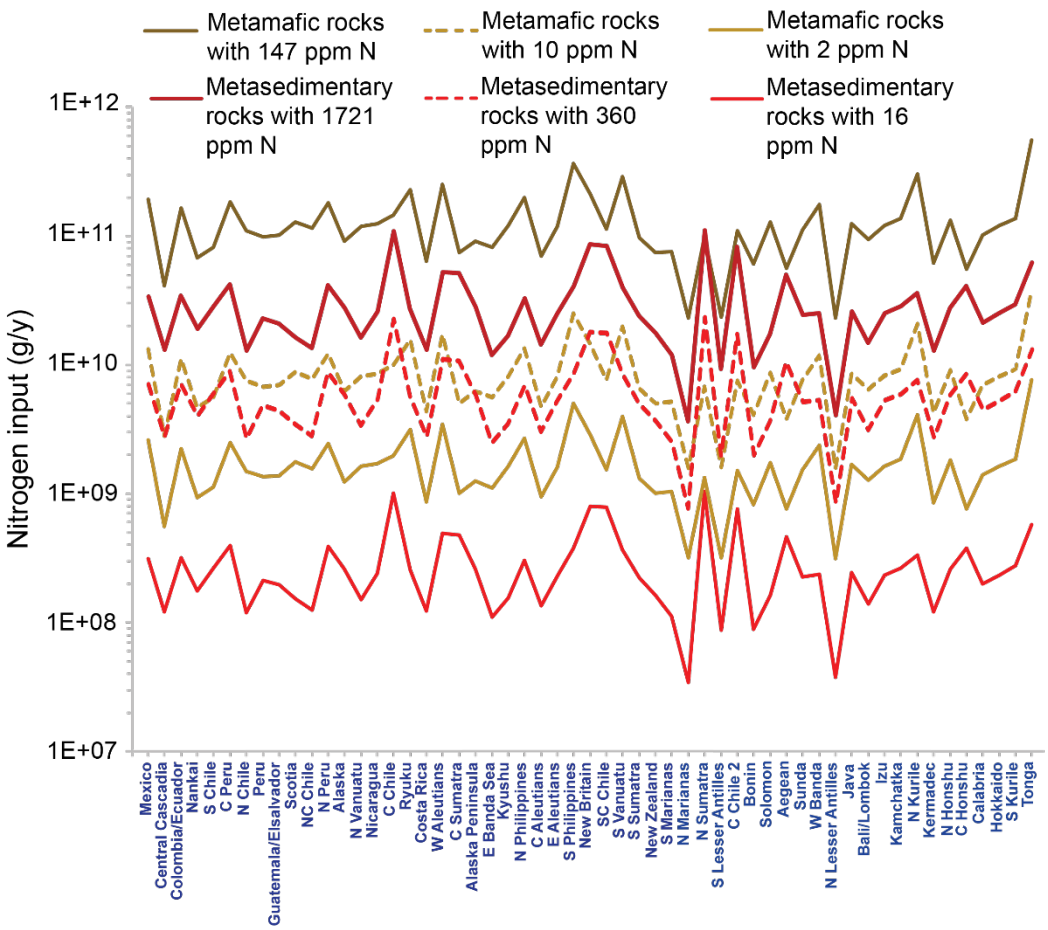

Figure 4. Nitrogen input fluxes (in grams/year) across 55 subduction zones today where the subduction zones are arranged from left to right according to decreasing slab-top temperatures at 100 km depth (based on model D80 of Syracuse et al., 2010).

We consider the maximum (147 ppm for metabasic rocks from this study; 1721 ppm for metasediments from Busigny et al., 2003), minimum (2 ppm for metabasic rocks from Halama et al., 2017; 16 ppm for metasedimentary rocks from Bebout, 1997) and median N concentrations (360 ppm for metasedimentary and 12 ppm for metabasic rocks) in the subducted lithologies to estimate the fluxes of N in subduction zones (Table S1). The reason why we consider the range in concentrations with the median rather than the standard deviations is explained as follows. The N concentrations reported in the literature (including this study) for metasediments and metabasic rocks display highly positively skewed distributions: 43% of the data from metasedimentary rocks have

concentrations within 266 ppm while 70% of the data from metabasic rocks lie within 22 ppm. Whether the skewed distributions represent the actual input across subduction zones globally or they are heavily biased by sampling is yet to be determined and highlights the importance of studying N behavior in metamorphic rocks in more locations globally. A fallout of the highly skewed distribution is that standard deviations are largely overestimated, hence, we use the range in the data to estimate fluxes. We do however acknowledge that until the validity of the skewness in distribution is established by future studies, it is more logical to use the median concentrations to better understand the overall deep cycling of N in subduction zones. The range of concentrations encompass a realm of possibilities including (a) some N could be lost by sediments during metamorphism and taken up by metabasic rocks, as supported by Halama et al., (2021), K. Li et al., (2021) and this study, so a closed system scenario where no net loss of N takes place from the system (b) N may be lost from the metasediments and metabasic rocks in the mélange by dehydration and fore-arc depth partial melting (for very hydrous sediments in hot subduction zones), so an open system scenario where net N loss takes place from the system. Therefore, the calculated N fluxes via metasedimentary rocks represent the rate of N input at forearc depths after the loss to metabasic rocks or from the system itself (where the system consists of metasediments and metabasic rocks). The calculated N fluxes for metabasic rocks represent the amount of N carried to forearc depths either after gaining from metasediments, or some N inherited during alteration on the seafloor (e.g. Halama et al., 2010a), or likely N lost from the system during metamorphic devolatilization (e.g. Halama et al., 2010a).

We find that for maximum and minimum N concentrations, the N input at forearc depths through metasediments are 1.74×10^{12} g/y and 1.62×10^{10} g/y respectively, and through metabasic rocks are 7.24×10^{12} g/y and 9.85×10^{10} g/y respectively. The N input fluxes via median concentrations of N are 3.65×10^{11} g/y and 5.91×10^{11} g/y for metasediments and metabasic rocks respectively. These fluxes imply that metabasic rocks, irrespective of their N contents, supply an overall higher flux of N at forearc depths than metasediments even though metasedimentary rocks have at least an order of magnitude higher N concentration than metabasic rocks.

The global median input flux of 5.91×10^{11} g/y for metabasic rocks in this study is similar to the input flux of 5.46×10^{11} g/y estimated by Busigny et al. (2011) (based on metabasic rocks from western Alps) but is higher than the input fluxes of $(2.9 – 4.2) \times 10^{11}$ g/y by unmetamorphosed mafic oceanic crust as reported by Li and Li (2023). This is due to the fact that the median concentrations of 12 ppm of N (this study) and 10.6 ppm (Busigny et al., 2011) in metabasic rocks used to estimate the above fluxes are higher than the N concentrations of 6.6 – 10.6 ppm in unmetamorphosed mafic oceanic crust assumed by (Li and Li, 2023a), likely representing the net gain of N in mafic rocks from their sedimentary counterparts during metamorphism. This is supported by the overall decrease in median concentration of N from unmetamorphosed sediments (790 ppm with a range from 5 – 2382 ppm; Sadofsky and Bebout, 2003; Li and Bebout, 2005a, b) to their metamorphosed equivalent (360 ppm with a range from 16-1721 ppm; Bebout and Fogel, 1992; Bebout, 1997; Busigny et al., 2003; Sadofsky and Bebout, 2003; Halama et al., 2010; Bebout et al., 2013; Cannaò et al., 2020).

The global N input flux at forearc and subsequently to sub-arc conditions via metasediments and metabasic rocks (assuming the median N concentrations in metasediments and metabasic rocks) is 9.55×10^{11} g/y. This flux is slightly higher than 8.69×10^{11} g/y as determined by Mallik et al., (2018) where they assumed the same subduction zone segments from (van Keken et al., 2011) and average N concentrations of 424 ppm in sediments (only 18% higher than the median concentration used in this study) and 6 ppm in mafic extrusives and gabbros (half of the median concentration used in this study). Factoring in sediments that are scraped off and not subducted would decrease the fluxes of N delivery by metasediments even further, thus not affecting the relative dominance of metabasic rocks in delivering N to forearc depths. Adding mafic rocks due to continental subduction would increase the fluxes of N supply to forearc depths by subduction of metabasic rocks and thus the relative dominance of metabasic rocks in N delivery would still hold. Nevertheless, the large variation in N abundance in metabasic rocks in this study highlight the need to further investigate more metabasic rocks from locations worldwide to obtain a more robust estimate of N inputs by metabasic rocks.

6. Concluding remarks and future directions

We investigate the N abundance, isotope compositions and trace element characteristics of amphibolites and epidote-blueschists from the Central Qiangtang Metamorphic Belt in Tibet which likely represent mafic rocks from the transition of oceanic to continental subduction. We find that the rocks acquired N from sedimentary

or continental fluids during metamorphism either within the subduction channel or during underthrusting. We estimate the fluxes of N in modern-day subduction zones by metasedimentary and metabasic rocks and find that metabasic rocks are the dominant carriers of N to subduction zones which reinforces the need to investigate the behavior of N in metabasic rocks better for an improved understanding of global deep N cycling.

The fact that N in metabasic rocks from different locations globally show different scenarios of N behavior pre- and post-subduction highlight the importance of investigating a wider array of metabasic rocks from locations worldwide and that N behavior inferred from a few locations may not be representative of N deep cycling at a planetary scale. This highlights the need for investigation of N characteristics in metabasic rocks from more locations to improve our understanding of deep N cycling due to subduction.

With the revised input fluxes reported in this study, future studies need to re-evaluate the fluxes that are released from the subducting slab and their potential controlling factors (e.g., thermal structure) in individual subduction zones worldwide (Mallik et al., 2018; Förster et al., 2019; Jackson et al., 2021; Li and Li, 2022) to better constrain the N budgets during deep cycling. Constraining fluxes out of the slab requires detailed phase equilibria studies for the various mélange lithologies especially the mode and stability of key N hosting minerals, along with fluid-mineral and melt-mineral partition coefficients of N as a function of pressure, temperature and oxygen fugacity applicable for subducted slabs.

Acknowledgements

The authors acknowledge Zachary Michels for assistance with the SEM at Arizona Laserchron Center, Hamilton Analytical Laboratory for trace element analysis, Grindstone Laboratories for thin-section preparation, and Lisa Zieman for assistance with the shatterbox that was used for pulverizing samples. AM acknowledges National Science Foundation grant EAR 2138410, and her startup grant from the Office for Research, Innovation and Impact and Eminent Scholar Funds from the College of Science at the University of Arizona. AR acknowledges the David J. Lowell Scholarship from the University of Arizona. LL acknowledges an NSERC-Discovery Grant. PK acknowledges National Science Foundation grant EAR 2048656. EC acknowledges National Science Foundation grant EAR 2138484.

Data Availability

Data, including Supplementary Information, are available through University of Arizona Research Data Repository (ReDATA) at https://figshare.com/s/08ecf213aff5b5fcd022 .

References

Ague J. J. (2011) Extreme channelization of fluid and the problem of element mobility during Barrovian metamorphism. *Am. Mineral.* **96**, 333–352.

Bach W., Peucker-Ehrenbrink B., Hart S. R. and Blusztajn J. S. (2003) Geochemistry of hydrothermally altered oceanic crust: DSDP/ODP Hole 504B–Implications for seawater-crust exchange budgets and Sr-and Pb-isotopic evolution of the mantle.

515 *Geochemistry, Geophys. Geosystems* **4**.
516 Bebout G. E. (2007) Metamorphic chemical geodynamics of subduction zones. *Earth*
517 *Planet. Sci. Lett.* **260**, 373–393.
518 Bebout G. E. (1997) Nitrogen isotope tracers of high-temperature fluid-rock interactions:
519 Case study of the Catalina Schist, California. *Earth Planet. Sci. Lett.* **151**, 77–90.
520 Bebout G. E., Banerjee N. R., Izawa M. R. M., Kobayashi K., Lazzeri K., Ranieri L. A.
521 and Nakamura E. (2018) Nitrogen Concentrations and Isotopic Compositions of
522 Seafloor-Altered Terrestrial Basaltic Glass: Implications for Astrobiology.
523 *Astrobiology* **18**, 330–342.
524 Bebout G. E. and Barton M. D. (2002) Tectonic and metasomatic mixing in a high-T,
525 subduction-zone mélange - Insights into the geochemical evolution of the slab-
526 mantle interface. *Chem. Geol.* **187**, 79–106.
527 Bebout G. E. and Fogel M. L. (1992) Nitrogen-isotope compositions of metasedimentary
528 rocks in the Catalina Schist, California: Implications for metamorphic
529 devolatilization history. *Geochim. Cosmochim. Acta* **56**, 2839–2849.
530 Bebout G. E., Fogel M. L. and Cartigny P. (2013) Nitrogen: Highly Volatile yet
531 Surprisingly Compatible. *Elements* **9**, 333–338.
532 Beinlich A., Klemd R., John T. and Gao J. (2010) Trace-element mobilization during Ca-
533 metasomatism along a major fluid conduit: Eclogitization of blueschist as a
534 consequence of fluid-rock interaction. *Geochim. Cosmochim. Acta* **74**, 1892–1922.
535 Bucher-Nurminen K. (1987) A recalibration of the chlorite-biotite-muscovite
536 geobarometer. *Contrib. to Mineral. Petrol.* **96**, 519–522.
537 Busigny V. and Bebout G. E. (2013) Nitrogen in the silicate earth:Speciation and

isotopic behavior during mineral-fluid interactions. *Elements* **9**, 353–358.

Busigny V., Cartigny P., Laverne C., Teagle D., Bonifacie M. and Agrinier P. (2019) A re-assessment of the nitrogen geochemical behavior in upper oceanic crust from Hole 504B: Implications for subduction budget in Central America. *Earth Planet. Sci. Lett.* **525**, 115735.

Busigny V., Cartigny P. and Philippot P. (2011) Nitrogen isotopes in ophiolitic metagabbros: A re-evaluation of modern nitrogen fluxes in subduction zones and implication for the early Earth atmosphere. *Geochim. Cosmochim. Acta* **75**, 7502–7521.

Busigny V., Cartigny P., Philippot P., Ader M. and Javoy M. (2003) Massive recycling of nitrogen and other fluid-mobile elements (K, Rb, Cs, H) in a cold slab environment: evidence from HP to UHP oceanic metasediments of the Schistes Lustrés nappe (western Alps, Europe). *Earth Planet. Sci. Lett.* **215**, 27–42.

Busigny V., Chen J., Philippot P., Borensztajn S. and Moynier F. (2018) Insight into hydrothermal and subduction processes from copper and nitrogen isotopes in oceanic metagabbros. *Earth Planet. Sci. Lett.* **498**, 54–64.

Busigny V., Laverne C. and Bonifacie M. (2005) Nitrogen content and isotopic composition of oceanic crust at a superfast spreading ridge: A profile in altered basalts from ODP Site 1256, Leg 206. *Geochemistry, Geophys. Geosystems* **6**.

Cannaò E., Tiepolo M., Bebout G. E. and Scambelluri M. (2020) Into the deep and beyond: Carbon and nitrogen subduction recycling in secondary peridotites. *Earth Planet. Sci. Lett.* **543**, 116328.

Cooperdock E. H. G., Raia N. H., Barnes J. D., Stockli D. F. and Schwarzenbach E. M.

(2018) Tectonic origin of serpentinites on Syros, Greece: Geochemical signatures of abyssal origin preserved in a HP/LT subduction complex. *Lithos* **296**–**299**, 352–364.

Dan W., Wang Q., White W. M., Zhang X. Z., Tang G. J., Jiang Z. Q., Hao L. L. and Ou Q. (2018) Rapid formation of eclogites during a nearly closed ocean: Revisiting the Pianshishan eclogite in Qiangtang, central Tibetan Plateau. *Chem. Geol.* **477**, 112–122.

Ducea M. N. (2016) RESEARCH FOCUS: Understanding continental subduction: A work in progress. *Geology* **44**, 239–240.

Förster M. W., Foley S. F., Alard O. and Buhre S. (2019) Partitioning of nitrogen during melting and recycling in subduction zones and the evolution of atmospheric nitrogen. *Chem. Geol.* **525**, 334–342.

Gale A., Dalton C. A., Langmuir C. H., Su Y. and Schilling J. G. (2013) The mean composition of ocean ridge basalts. *Geochemistry, Geophys. Geosystems* **14**, 489–518.

Halama R., Bebout G. E. and Bea F. (2021) Nitrogen loss and isotopic fractionation during granulite-facies metamorphism in the lower crust (Ivrea Zone, NW Italy). *Chem. Geol.*, 120475.

Halama R., Bebout G. E., John T. and Schenk V. (2010) Nitrogen recycling in subducted oceanic lithosphere: The record in high- and ultrahigh-pressure metabasaltic rocks. *Geochim. Cosmochim. Acta* **74**, 1636–1652.

Halama R., Bebout G. E., Marschall H. R. and John T. (2017) Fluid-induced breakdown of white mica controls nitrogen transfer during fluid–rock interaction in subduction

584 zones. *Int. Geol. Rev.* **59**, 702–720.
585 Harris B. J. R., de Hoog J. C. M. and Halama R. (2022) The behaviour of nitrogen
586 during subduction of oceanic crust: Insights from in situ SIMS analyses of high-
587 pressure rocks. *Geochim. Cosmochim. Acta* **321**, 16–34.
588 Holland T. and Blundy J. (1994) Non-ideal interactions in calcic amphiboles and their
589 bearing on amphibole-plagioclase thermometry. *Contrib. to Mineral. Petrol.* **116**,
590 433–447.
591 Jackson C. R. M., Cottrell E. and Andrews B. (2021) Warm and oxidizing slabs limit
592 ingassing efficiency of nitrogen to the mantle. *Earth Planet. Sci. Lett.* **553**, 116615.
593 Jarrard R. D. (2003) Subduction fluxes of water, carbon dioxide, chlorine, and
594 potassium. *Geochemistry, Geophys. Geosystems* **4**.
595 Jochum K. P., Weis U., Schwager B., Stoll B., Wilson S. A., Haug G. H., Andreae M. O.
596 and Enzweiler J. (2016) Reference Values Following ISO Guidelines for Frequently
597 Requested Rock Reference Materials. *Geostand. Geoanalytical Res.* **40**, 333–350.
598 John T., Scherer E. E., Haase K. and Schenk V. (2004) Trace element fractionation
599 during fluid-induced eclogitization in a subducting slab: Trace element and Lu-Hf-
600 Sm-Nd isotope systematics. *Earth Planet. Sci. Lett.* **227**, 441–456.
601 Johnson D. M., Hooper P. R. and Conrey R. M. (1999) XRF analysis of rocks and
602 minerals for major and trace elements on a single low dilution Li-tetraborate fused
603 bead. *Adv. X-ray Anal.* **41**, 843–867.
604 Kapp P. and Decelles P. G. (2019) Mesozoic–Cenozoic geological evolution of the
605 Himalayan-Tibetan orogen and working tectonic hypotheses. *Am. J. Sci.* **319**, 159–
606 254.

607 Kapp P., Yin A., Manning C. E., Harrison T. M., Taylor M. H. and Ding L. (2003)
608 Tectonic evolution of the early Mesozoic blueschist-bearing Qiangtang
609 metamorphic belt, central Tibet. *Tectonics* **22**.
610 Kapp P., Yin A., Manning C. E., Murphy M., Harrison T. M., Spurlin M., Lin D., Xi-Guang
611 D. and Cun-Ming W. (2000) Bluechist-bearing metamorphic core complexes in the
612 Qiangtang block reveal deep crustal structure of northern Tibet. *Geology* **28**, 19–
613 22.
614 Kastens K. A., Mascle J., Auroux C. and .... (1987) Site 650: Marsili Basin. In
615 *Proceedings of the Ocean Drilling Program, 107 Initial Reports* Ocean Drilling
616 Program.
617 van Keken P. E., Hacker B. R., Syracuse E. M. and Abers G. A. (2011) Subduction
618 factory: 4. Depth-dependent flux of H2O from subducting slabs worldwide. *J.*
619 *Geophys. Res. Solid Earth* **116**.
620 Kelley K. A., Plank T., Ludden J. and Staudigel H. (2003) Composition of altered
621 oceanic crust at ODP Sites 801 and 1149. *Geochemistry, Geophys. Geosystems* **4**.
622 King R. L., Kohn M. J. and Eiler J. M. (2003) Constraints on the petrologic structure of
623 the subduction zone slab-mantle interface from Franciscan Complex exotic
624 ultramafic blocks. *GSA Bull.* **115**, 1097–1109.
625 Kohn M. J. and Spear F. S. (1990) Two new geobarometers for garnet amphibolites,
626 with applications to southeastern Vermont. *Am. Mineral.* **75**, 89–96.
627 Li C., R. C., Hu K., Yu Z. and H. Y. (1995) Study on the Paleo-Tethys Suture Zone of
628 Lungmu Co-Shuanghu, Tibet. *Geol. Publ. House, Beijing, China*.
629 Li K., Li G.-Y., Du Y.-F., Han W., Zhang J., Chen L.-H., Zhou J.-B. and Li L. (2021)

630 Intraslab remobilization of nitrogen during early subduction facilitates deep nitrogen
631 recycling: Insights from the blueschists in the Heilongjiang Complex in NE China.
632 *Chem. Geol.* **583**, 120474.
633 Li K. and Li L. (2023a) Alteration enrichment of nitrogen in the gabbroic oceanic crust:
634 Implications for global subducting nitrogen budget and subduction-zone nitrogen
635 recycling. *Geochim. Cosmochim. Acta* **351**, 96–107.
636 Li K. and Li L. (2023b) Nitrogen enrichment in the altered upper oceanic crust: A new
637 perspective on constraining the global subducting nitrogen budget and implications
638 for subduction-zone nitrogen recycling. *Earth Planet. Sci. Lett.* **602**, 117960.
639 Li K. and Li L. (2022) Nitrogen enrichments in sheeted dikes and gabbros from
640 DSDP/ODP/IODP Hole 504B and 1256D: Insights into nitrogen recycling in Central
641 America and global subduction zones. *Geochim. Cosmochim. Acta* **335**, 197–210.
642 Li L. and Bebout G. E. (2005a) Carbon and nitrogen geochemistry of sediments in the
643 Central American convergent margin: Insights regarding subduction input fluxes,
644 diagenesis, and paleoproductivity. *J. Geophys. Res. Solid Earth* **110**, B11202.
645 Li L. and Bebout G. E. (2005b) Carbon and nitrogen geochemistry of wedge sediments
646 at odp site 1040: Evidence for sediment sources, diagenetic history, and fluid
647 mobility. In *Proceedings of the Ocean Drilling Program: Scientific Results* Texas A
648 & M University. pp. 1–38.
649 Li L., Bebout G. E. and Idleman B. D. (2007) Nitrogen concentration and δ15N of
650 altered oceanic crust obtained on ODP Legs 129 and 185: Insights into alteration-
651 related nitrogen enrichment and the nitrogen subduction budget. *Geochim.*
652 *Cosmochim. Acta* **71**, 2344–2360.

Li L., He Y., Zhang Z. and Liu Y. (2021a) Nitrogen isotope fractionations among gaseous and aqueous NH4+, NH3, N2, and metal-ammine complexes: Theoretical calculations and applications. *Geochim. Cosmochim. Acta* **295**, 80–97.

Li L., Li K., Li Y., Zhang J., Du Y. and Labbe M. (2021b) Recommendations for offline combustion-based nitrogen isotopic analysis of silicate minerals and rocks. *Rapid Commun. Mass Spectrom.* **35**, e9075.

Liang X., Wang G., Yang B., Ran H., Zheng Y., Du J. and Li L. (2017) Stepwise exhumation of the triassic lanling high-pressure metamorphic belt in central Qiangtang, Tibet: Insights from a coupled study of metamorphism, deformation, and geochronology. *Tectonics* **36**, 652–670.

Mallik A., Li Y. and Wiedenbeck M. (2018) Nitrogen evolution within the Earth's atmosphere–mantle system assessed by recycling in subduction zones. *Earth Planet. Sci. Lett.* **482**.

Massonne H. J. and Schreyer W. (1987) Phengite geobarometry based on the limiting assemblage with K-feldspar, phlogopite, and quartz. *Contrib. to Mineral. Petrol.* **96**, 212–224.

Plank T. and Langmuir C. H. (1998) The chemical composition of subducting sediment and its consequences for the crust and mantle. *Chem. Geol.* **145**, 325–394.

Powell R. and Evans J. A. (1983) A new geobarometer for the assemblage biotite-muscovite-chlorite-quartz. *J. Metamorph. Geol.* **1**, 331–336.

Pullen A., Kapp P., Gehrels G. E., Vervoort J. D. and Ding L. (2008) Triassic continental subduction in central Tibet and Mediterranean-style closure of the Paleo-Tethys Ocean. *Geology* **36**, 351–354.

676 Sadofsky S. J. and Bebout G. E. (2003) Record of forearc devolatilization in low-T, high-
677 P/T metasedimentary suites: Significance for models of convergent margin
678 chemical cycling. *Geochemistry, Geophys. Geosystems* **4**.
679 Seyfried W. E., Chen X. and Chan L. H. (1998) Trace element mobility and lithium
680 isotope exchange during hydrothermal alteration of seafloor weathered basalt: an
681 experimental study at 350°C, 500 bars. *Geochim. Cosmochim. Acta* **62**, 949–960.
682 Shannon R. D. (1976) Revised effective ionic radii and systematic studies of interatomic
683 distances in halides and chalcogenides. *Acta Crystallogr. Sect. A* **32**, 751–767.
684 Sidey V. (2016) On the effective ionic radii for ammonium. *Acta Crystallogr. Sect. B*
685 *Struct. Sci. Cryst. Eng. Mater.* **72**, 626–633.
686 Sorensen S. S., Grossman J. N. and Perfit M. R. (1997) Phengite-hosted LILE
687 enrichment in eclogite and related rocks: Implications for fluid-mediated mass
688 transfer in subduction zones and arc magma genesis. *J. Petrol.* **38**, 3–34.
689 van der Straaten F., Halama R., John T., Schenk V., Hauff F. and Andersen N. (2012)
690 Tracing the effects of high-pressure metasomatic fluids and seawater alteration in
691 blueschist-facies overprinted eclogites: Implications for subduction channel
692 processes. *Chem. Geol.* **292**–**293**, 69–87.
693 Sun S. S. and McDonough W. F. (1989) Chemical and isotopic systematics of oceanic
694 basalts: Implications for mantle composition and processes. *Geol. Soc. Spec. Publ.*
695 **42**, 313–345.
696 Syracuse E. M., van Keken P. E. and Abers G. A. (2010) The global range of
697 subduction zone thermal models. *Phys. Earth Planet. Inter.* **183**, 73–90.
698 Wu H., Li C., Chen J. and Xie C. (2016) Late Triassic tectonic framework and evolution

of Central Qiangtang, Tibet, SW China. *Lithosphere* **8**, 141–149.

Xu W., Liu F., Zhai Q. and Dong Y. (2021) Petrology and P–T path of blueschists from central Qiangtang, Tibet: Implications for the East Paleo-Tethyan evolution. *Gondwana Res.* **94**, 12–27.

Zhai Q. G., Jahn B. M., Zhang R. Y., Wang J. and Su L. (2011) Triassic Subduction of the Paleo-Tethys in northern Tibet, China: Evidence from the geochemical and isotopic characteristics of eclogites and blueschists of the Qiangtang Block. *J. Asian Earth Sci.* **42**, 1356–1370.

Zhang K. J., Cai J. X., Zhang Y. X. and Zhao T. P. (2006) Eclogites from central Qiangtang, northern Tibet (China) and tectonic implications. *Earth Planet. Sci. Lett.* **245**, 722–729.

Zhang X. Z., Dong Y. S., Wang Q., Dan W., Zhang C., Xu W. and Huang M. L. (2017) Metamorphic records for subduction erosion and subsequent underplating processes revealed by garnet-staurolite-muscovite schists in central Qiangtang, Tibet. *Geochemistry, Geophys. Geosystems* **18**, 266–279.